Transaction B: Mechanical Engineering
Vol. 16, No. 2, pp. 149–158

SCIENTIA IRANICA

The Effect of Wake Flow and Skew Angle on the Ship Propeller Performance

H. Ghassemi[1]

Abstract. *This paper provides an investigation into the influence of wake and skew on a ship propeller performance, based on the potential Boundary Element Method (BEM). Two types of inflow wake from a ship (i.e. Seiun-Maru and MS689) have been investigated for two propeller types; a Conventional Propeller (CP) and a Highly Skewed Propeller (HSP). The computed results include pressure distribution, open water characteristics and thrust fluctuation for one blade and for all blades of the propeller. Calculations of the unsteady pressure distributions, thrust and torque are in good agreement with experimental data. In addition, the effect of propeller skew angle on the performance of thrust and torque, is investigated.*

Keywords: *Skewed propeller; Inflow wake; Hydrodynamic performance.*

INTRODUCTION

Propellers usually operate in the ship's stern, where the inflow wake generates periodic and fluctuating pressure, due to which, as a result, vibratory forces can occur. The induced forces may transfer to the ship's hull directly via the shaft-line or indirectly through the fluid. Therefore, conditions for the crew and passengers become unpleasant and uncomfortable. The inflow wake is strongly dependent on the shape of the ship hull and, so, each ship may have a unique wake field. It is a great challenge for naval architects and hydro-dynamicists to predict the performance of ship propellers working at the stern of the ship hull.

Modern research in computational hydrodynamics is related to the development of the computer and to many numerical methods developed during the second half of the twentieth century. Among numerical tools, the potential-based Boundary Element Method (BEM) is strongly suitable for the analysis of any complex propeller configuration, because it has good accuracy combined with low computational time [1]. There are varieties of potential-based element methods, which employ different types of surface element, singularity distributions and boundary conditions. Most element methods are based on the Douglas Newmann constant source method, developed by Hess and Smith [2], in which the major unknown was the source strength, which is determined from the boundary condition of zero normal velocity at a control point on each element. Another formula has arisen from the application of Green's identity to determine unknown potential strength. Morino [3] first introduced it for the general lifting of bodies in the field of wing theory, using the hyperboloidal element. In past years, many researchers, such as Lee and Kinnas [4], Hoshino [5], Lee [6], Koyama [7], Ghassemi et al. [8-9] and Hsin [10], have applied this method to ship propeller problems in steady and unsteady flow, without the effect of the ship wake. Recently, the effect of a number of blades on wake evolution, for three propellers having the same blade geometry but a different number of blades, as well as the effect of wake flow were investigated [11,12].

In this paper, the author has tackled an accurate interpolated inflow wake, using a potential-based boundary element method applied to the hydrodynamic analysis of ship propellers operating in the inflow wake. Hyperboloidal quadrilateral elements, with constant source and dipole distributions, are also used to approximate the surface of the propeller. Furthermore, an Iterative Pressure Kutta (IPK) condition (with special numerical techniques) has been applied to satisfy pressure equality at the trailing edge, at each time step.

In this work, two different types of inflow wake, behind the ship hull (Seiun Maru, MS689), encountered two propeller types. The numerical results include

1. *Department of Marine Technology, Amirkabir University of Technology, Tehran, P.O. Box 15875-4413, Iran. E-mail: gasemi@aut.ac.ir*

Received 18 February 2007; received in revised form 25 July 2007; accepted 1 December 2007

pressure distribution, the open water characteristics of the propeller and the oscillating thrust and torque of the propellers (one blade and all blades) in one cycle. Most importantly, the results of the effect of skew angle on the hydrodynamic performance of two propeller types against the wake flow, are also investigated. A comparison of the present method with experimental data and Hoshino's computed method shows a good agreement [5,13,14].

MATHEMATICAL FORMULATIONS

Wake Flow onto the Propeller

In order to proceed with the Boundary Element Method (BEM), the total unsteady velocity potential, $\Phi(x,y,z,t)$, and the perturbation velocity potential, $\phi(x,y,z,t)$, are related as follows:

$$\Phi(x,y,z,t)=\Phi_I(x,y,z,t)+\phi(x,y,z,t), \tag{1}$$

where $\Phi_I(x,y,z,t)$ is the local unsteady potential flow onto the propeller, which is expressed as:

$$\Phi_I(x,y,z,t)=\vec{V}_I(x,y,z,t).\vec{X}_P(t), \tag{2}$$

where $\vec{V}_I(x,y,z,t)$ and $\vec{X}(x,y,z,t)_P$ are the unsteady inflow velocity and position vector of the propeller, respectively. The propeller behind the ship hull is assumed to rotate with a constant rotating speed, n, around the X-axis, in a negative direction, θ, as depicted in Figure 1.

The inflow velocity, $\vec{V}_I(x,y,z,t)$, represents the components of the inflow velocity field, towards the propeller, in Cartesian coordinates, defined by:

$$\vec{V}_I(x,y,z,t)=\vec{V}_W(x,y,z,t)+\vec{\omega}\times\vec{r}(x,y,z,t),$$

where:

$$\vec{\omega}=2\pi\vec{n}. \tag{3}$$

The assumption at this point is that the flow is incompressible and non-viscous. In addition, the wake velocity, $V_W(x,y,z,t)$, is assumed to be the effective wake, which includes interactions between the vorticities of the inflow wake, with and without the propeller. The measured wake flow should be employed, in order to obtain the propeller performance. Having the measured wake flow, $w(x,y,z,t)$, and ship speed, V_S, the flow velocities onto the propeller, due to the wake, are expressed as follows:

$$V_W(x,y,z,t)=V_S(1-w(x,y,z,t)). \tag{4}$$

The wake field is strongly dependent on the shape of the ship's stern and on environmental conditions. It is very difficult to predict the wake of a ship numerically, which is a challenge for many researchers today.

Basic Formula

By applying Green's theorem, the perturbation velocity potential, $\phi(x,y,z,t)$, at any point, can be expressed by a distribution of the source and doublet on the boundary surface, S_B, as in:

$$2\pi\phi(p,t)=\int_{S_B}\left\{\phi(q,t)\frac{\partial}{\partial n_q}\left(\frac{1}{R(p;q,t)}\right)\right.$$
$$\left.\frac{\partial\phi(q,t)}{\partial n_q}\left(\frac{1}{R(p;q,t)}\right)\right\}ds$$
$$+\int_{S_W}\Delta\phi(q,t)\frac{\partial}{\partial n_q}\left(\frac{1}{R(p;q,t)}\right)ds, \tag{5}$$

where $R(p;q)$ is the distance from the field point, p, to the singularity point, q. This equation may be regarded as a representation of the velocity potential, in terms of a normal dipole distribution of strength, $\phi(p,t)$, on the body surface, S_B, a source distribution of strength, $\partial\phi/\partial n$, on S_B, and a normal dipole distribution of strength, $\Delta\phi(q,t)$, on the trailing sheet surface, S_W.

Boundary Conditions

The strength of the source distribution in Equation 5 is known from the Kinematic Boundary Condition

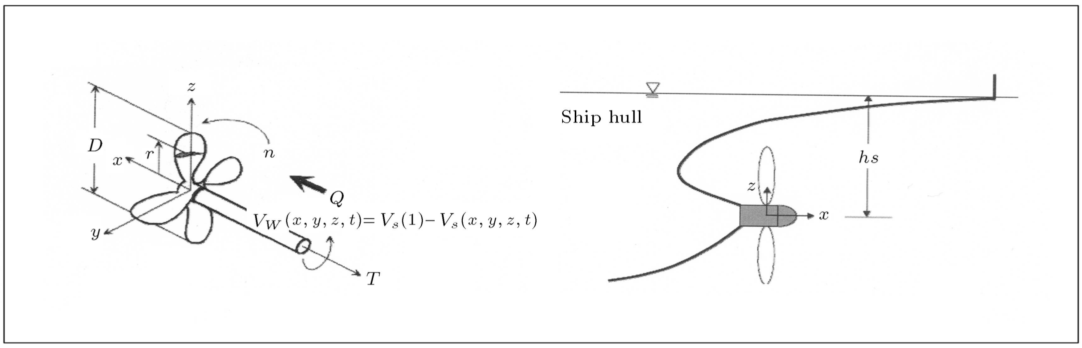

Figure 1. Coordinate system of propeller behind the ship hull.

(KBC), as follows:

$$\frac{\partial\phi}{\partial n} = -\vec{V}_I(x,y,z,t).\vec{n}$$
$$= -[V_S(1-w(x,y,z,t)) + \vec{\omega}\times\vec{r}(x,y,z,t)]\vec{n}, \quad (6)$$

where $\vec{n}$ denotes the outward normal unit vector. The strength of dipole distribution is unknown and is equal to the perturbation potential on the propeller or to the potential jump in the trailing sheet vortex. On the wake surface, S_W, the velocity is considered continuous, while the potential has a jump across the wake. The boundary condition on the surface S_W can be written as:

$$\Delta\left(\frac{\partial\phi(r,t)}{\partial n}\right)_{S_W} = \left(\frac{\partial\phi(r,t)}{\partial n}\right)^B - \left(\frac{\partial\phi(r,t)}{\partial n}\right)^F = 0, \quad (7)$$

and:

$$(\Delta\phi(r,t))_{S_W} = \phi^B(r,t) - \phi^F(r,t) = \Gamma(r,t), \quad (8)$$

where indices B and F refer to the back and face sides of the propeller, respectively.

In the steady flow problem, the potential jump, $\Delta\phi(q)$, is constant across the wake surface along an arbitrary streamline in the wake and its value is also constant with time, but when the unsteady flow is streamed along the trailing sheet, the value of the potential varies with time.

Another important physical boundary condition is the Kutta condition and its implementation. In lifting flows, the circulation distribution on the lifting portions drives the entire solution. Accordingly, accurate determination of this circulation is crucial. The values of the circulation are determined mainly from the Kutta condition along the trailing edges and, thus, specifications of the Kutta condition are more important than any other detail of the numerical implementation.

The theoretical and physical form of the Kutta condition states that the velocity shall remain finite all along the sharp trailing edges. An equivalent alternative form may be imposed on the numerical solution, such that equal pressure occurs on the back and front surfaces of the trailing edge. This equal pressure Kutta condition is applied to determine the unknown $\Delta\phi_{TE}$ of the dipole strength on the wake surface. In the numerical calculation, the pressure Kutta condition is expressed as:

$$\Delta p_{TE}(r,t) = p^B_{TE}(r,t) - p^F_{TE}(r,t) = 0. \quad (9)$$

A direct solution of the resulting system of equations obtained from the discretized Green's formula for the perturbation velocity potential (Equation 5), along with Kutta condition (Equation 9), is difficult, due to the nonlinear character of Equation 5. Therefore, an iterative solution algorithm is employed to solve the problem [11]. We focus on the numerical implementation in the following section.

NUMERICAL IMPLEMENTATION

The body surface is discretized by quadrilateral hyperboloidal elements represented by four vortices, which may not constitute a plane but which are still connected with straight lines. At the centroid of each element, a local coordinate system is defined choosing two tangential vectors, with respect to chordwise and spanwise. The third axis is the local normal vector obtained as a vector product of the two tangential vectors. The centroid is also chosen as the collocation point, where one should compute the influence coefficients and satisfy the boundary conditions. The trailing sheet vortex surface may be treated by a different approach, but we may assume, for simplicity, that hyperboloidal elements also cover it.

To solve Equation 5 numerically, the discretization of the propeller and its trailing sheet vortex surfaces are detailed into quadrilateral elements. The time domain is also discretized into equal intervals, Δt. The trailing sheet vortex starts from the blade trailing edge and flows downstream of the propeller along the prescribed helical surface, by interval $\Delta\theta_W$, as follows:

$$\Delta\theta_W = \omega\Delta t. \quad (10)$$

On each of the quadrilateral elements, the dipole and source distributions are approximated by constant strength distributions. Discretization of Equation 5 leads to a linear system of algebraic equations for the unknown ϕ at each time step, $L = t/\Delta t$, as:

$$2\pi\phi_i(L) = \sum_{k=1}^{K}\sum_{j=1}^{N_{\mathrm{tot}}} D^k_{ij}(\phi^k_j(L))$$
$$+ \sum_{k=1}^{K}\sum_{j=1}^{M}\sum_{l=1}^{N_W} W^k_{ijl}(\Delta\phi^k_j(L))$$
$$+ \sum_{k=1}^{K}\sum_{j=1}^{N_{\mathrm{tot}}} S^k_{ij}\left(\frac{\partial\phi}{\partial n}\right)^k j(L),$$
$$i = 1, 2, \cdots, N_{\mathrm{tot}}, \quad (11)$$

where D^k_{ij}, W^k_{ijl} (dipole distributions on body and wake surfaces) and S^k_{ij} (source distribution on body) are influence coefficients on the element, j, acting on the control point of element, i. These coefficients are analytically evaluated by Morino [4]. The use of quadrilateral surface elements, instead of planar elements, has been found to be important for the convergence of the present potential based boundary element method. It is discovered, particularly, when the method is applied to a highly skewed propeller and a twisted shape.

The systems of Equation 11 is solved, at each time step, L, with respect to the potentials on all blades. Nevertheless, the influence coefficients are determined on the key blade and re-arranged for all blades in the full matrix form.

It was found that 60 time steps per revolution of the propeller, $\Delta\theta_W = 6$ degrees, was enough and the results were accurate, although the results could be improved if the number of time steps was increased to 120 (i.e. $\Delta\theta_W = 3$ degrees). However, the effect of the angular interval, $\Delta\theta_W$, on the calculation of the thrust of one blade was not great. Therefore, the angular interval of 6 degrees is commonly used in the present calculations.

Hydrodynamic Forces Due to Inflow Wake

Once the perturbation potential is found, the perturbation tangential velocity, $\vec{v}_t(t)$, can be determined by a derivative of the potential. Then, unsteady pressure distribution on the propeller blade is calculated by the unsteady Bernoulli equation, expressed as:

$$p(t)=p_\infty+0.5\rho(2V_l(t).\vec{v}_t(t)-\vec{v}_t(t).\vec{v}_t(t))-\rho\frac{\partial\phi(t)}{\partial t}, \tag{12}$$

where p_∞ is the upstream hydrostatic pressure, $V_I(t)$ is the inflow velocity into the propeller found from Equation 3. The time derivative of the potential, $\partial\phi/\partial t$, in Equation 12, is inherent in the unsteady flow and can be obtained by a second order backward difference scheme as [1]:

$$\frac{\Delta\phi}{\Delta t} = \frac{4\phi(L) - 3\phi(L-1) + \phi(L-2)}{2\Delta t}. \tag{13}$$

The pressure coefficient is determined as follows:

$$C_p = \frac{p(t) - p_\infty}{1/2\rho n^2 D^2}, \tag{14}$$

where n is the propeller rotating speed and D is the propeller diameter.

The unsteady forces, (F_x, F_y, F_z), and moments, (M_x, M_y, M_z), acting on a propeller can be obtained by integrating the unsteady pressures over the blade and hub surfaces. They are expressed on the fixed coordinate system, (x, y, z), as:

$$F_x(t) = -T(t) = \int_S (p(t) - p_\infty) n_x ds,$$

$$F_y(t) = \int_S (p(t) - p_\infty)(n_y \cos(\omega t) - n_z \sin(\omega t))ds,$$

$$F_z(t) = \int_S (p(t) - p_\infty)(n_z \cos(\omega t) - n_y \sin(\omega t))ds,$$

$$M_x(t) = Q(t) = \int_S (p(t) - p_\infty)(n_y z - n_z y)ds,$$

$$M_y(t) = \int_S (p(t) - p_\infty)[(n_z x - n_x z)\cos(\omega t) + (n_x y - n_y x)\sin(\omega t))]ds,$$

$$M_z(t) = \int_S (p(t) - p_\infty)[(n_x y - n_y x)\cos(\omega t) + (n_x z - n_z x)\sin(\omega t))]ds, \tag{15}$$

where $\vec{n}(n_x, n_y, n_z)$ is the outward normal vector on the propeller. $T(t)$ and $Q(t)$ are the thrust and torque of the propeller.

By adding the viscous components to the above forces and moments given by Prandtl-Schlichting formulas [5], we finally obtain the total unsteady propeller forces and moments. Then, the non-dimensional coefficients of the unsteady propellers, forces and moments are expressed as follows:

$$K_t(t) = \frac{T(t)}{\rho n^2 D^4}, \qquad K_q(t) = \frac{Q(t)}{\rho n^2 D^5},$$

$$K_{F_y}(t) = \frac{F_y(t)}{\rho n^2 D^4}, \qquad K_{M_y}(t) = \frac{M_y(t)}{\rho n^2 D^5},$$

$$K_{F_z}(t) = \frac{F_z(t)}{\rho n^2 D^4}, \qquad K_{M_z}(t) = \frac{M_z(t)}{\rho n^2 D^5}. \tag{16}$$

In the steady calculations, the hydrodynamic characteristics of the propeller are obtained as given below:

$$J = \frac{V_W(x)}{nD}, \quad K_t = \frac{T}{\rho n^2 D^4}, \quad K_q = \frac{Q}{\rho n^2 D^5}, \tag{17}$$

where $V_W(x)$ is the axial flow velocity into the propeller, which is called advance velocity, (V_A).

NUMERICAL RESULTS AND DISCUSSION

Propeller Type

In order to evaluate the accuracy and applicability of the present method, two different propeller types are examined. For both propellers, very precise measurements of the blade surface pressure are conducted. Both propellers have five blades. One is a conventional design with MAU sections and the other is a highly skewed propeller with modified SRI-b sections. Principal particulars of the propellers are shown in Table 1.

Table 1. Main dimensions of the propellers.

Propeller Type	Conventional Prop. (CP)	Highly Skewed Prop. (HSP)
Diameter (full scale) (m)	3.6	3.6
Exp. area ratio	0.65	0.70
Pitch ratio at 0.7R	0.95	0.944
Boss ratio	0.1972	0.1972
No. of blades	5	5
Blade thickness ratio	0.0442	0.0496
Rake angle (deg)	6.0	-3.03
Skew angle (deg)	10.5	45.0
Blade section	MAU	Modified SRI-B

Each blade of the propeller was discretized with (M = 12) in a radial and (N = 14) in a chordwise direction, so that the total number of elements was 336, plus a hub with (4^*28 = 112) elements per segment. The total number of elements for the steady calculation was 448 on the key blade. Hoshino [5] also selected the same element number in his research and he reached the conclusion that it is enough to get reasonable results. Although larger numbers of elements may be better, due to limited computer memory, the usage of high numbers of elements is not possible. The potential and pressure distributions on the other blades are taken as equal to the key blade. Figure 2 shows the element arrangements of the two propellers. In addition, the element arrangement for a HSP propeller and its trailing sheet vortex are shown in Figure 3.

For unsteady flow, each blade is subject to a different inflow wake velocity; the potential and pressure distributions are calculated at each time step. The system of equations is K times larger than the steady flow. Nevertheless, the element patterns kept the same as for the steady condition, which gave the total number of elements for all blades and hubs to be 2240. The CPU time for these element calculations (at one operating condition) was about 8 hours, using a PC Pentium 3.2 GHz processor for 180 time steps (three revolutions of the propeller). Because, at the same time, each propeller blade encountered the ship's wake flow, the Kutta condition should be applied to all blades at each time step. Therefore, most of the CPU time was for the convergence of the Kutta condition at the trailing edge. It was noted that, at each iterative Kutta condition, the system of equations should be solved $K^*M(5^*12 = 60)$ times at each time step. It is expected that the Kutta condition will be very time consuming in the unsteady flow. In the following sub-section, the numerical results for the steady and unsteady flows are discussed.

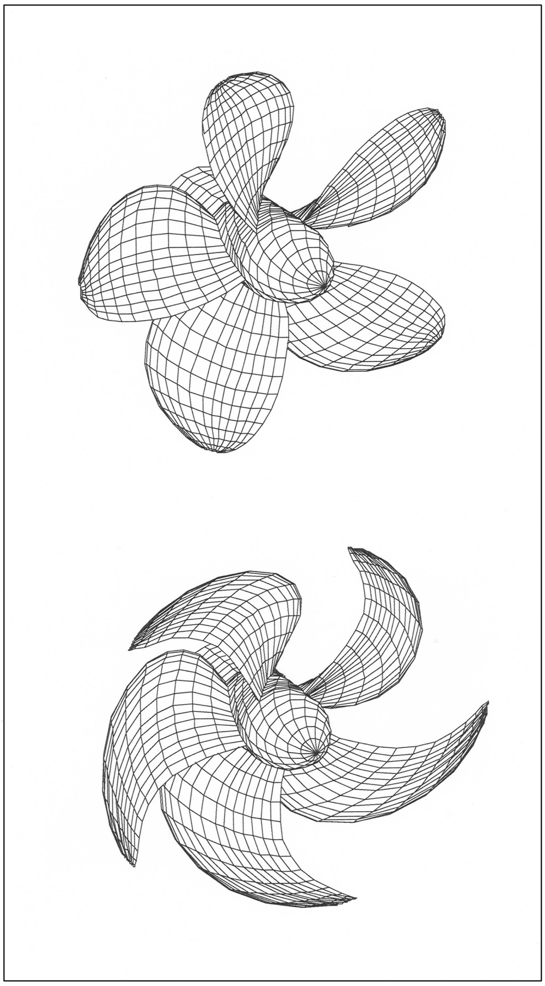

Figure 2. Element arrangement of CP (up) and HSP (down) propellers.

Inflow Wake

Data for the same propellers (but in full-scale) of CP and HSP were obtained in full-scale condition at the rear of the ship's hull, which was carried out by Ukon et al. [13] at the Ship Research Institute (presently named the National Maritime Research Center, in Japan). All principal particulars of both propellers are the same as the model, except the diameter, as given in Table 1. The measured effective wake flow contours indicate the axial speed of water, in fractions of the ship speed and the arrows indicate the transverse velocity field in front of the propeller, in full scale, as shown in

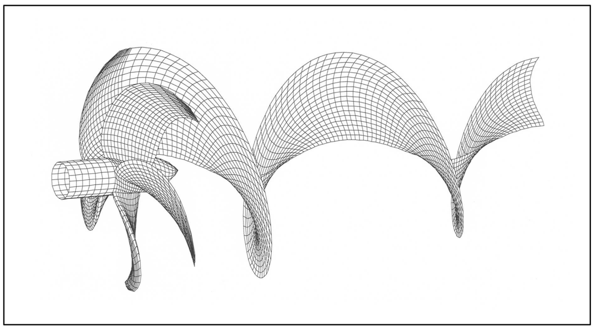

Figure 3. Element arrangement for a HSP propeller and its trailing sheet vortex.

Figure 4. In the present calculations, not only the axial flow component, but also the tangential and radial flow components, are taken into consideration. In our numerical code, the Spline interpolation method has been implemented to calculate the wake flow on each element of the propeller blades and hub, which measured the wake flow given by Ukon et al. [13]. Therefore, Figure 5 shows the interpolation wake flow behind the ship hull. Additionally, to show more on the wake and its interpolation, another wake is shown in Figure 6. This figure shows the inflow velocity (cross velocity is shown by the vector and the axial is shown by the counter forms) distribution behind the ship (MS689). In addition, another form of inflow velocity is shown in Figure 7 for each component of V_x, V_y, and V_z. The effects of two inflow ship wakes on each propeller (CP and HSP) have been investigated.

The element arrangement of the HSP propeller and its trailing sheet vortex is shown in Figure 3. In this case, the blade element calculations are also performed on both propellers (HSP and CP), with 14

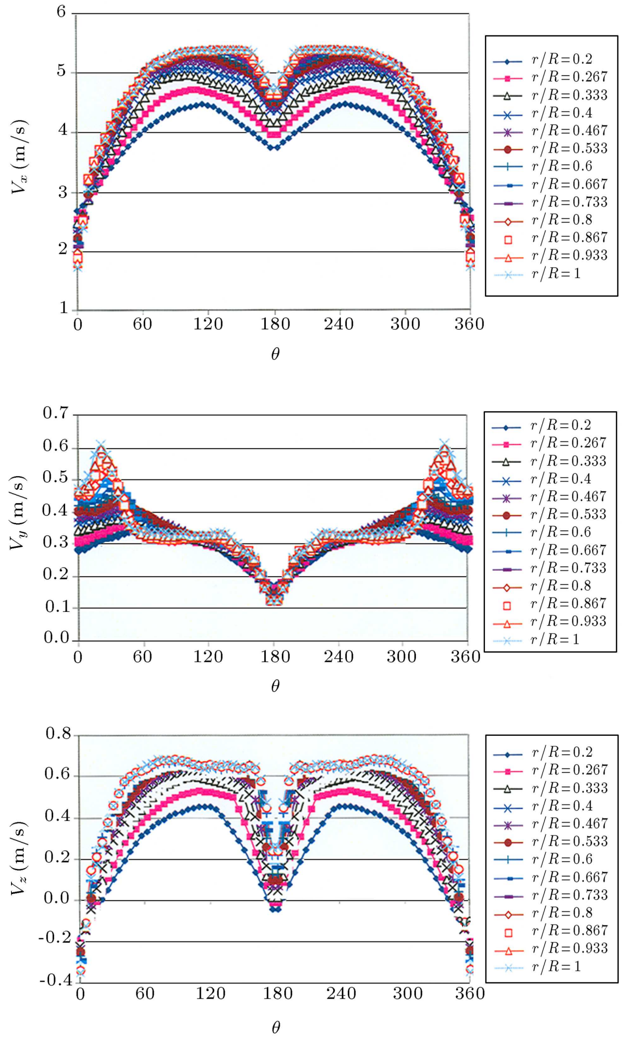

Figure 5. Interpolation of the inflow wake velocity for Seiun-Maru ship.

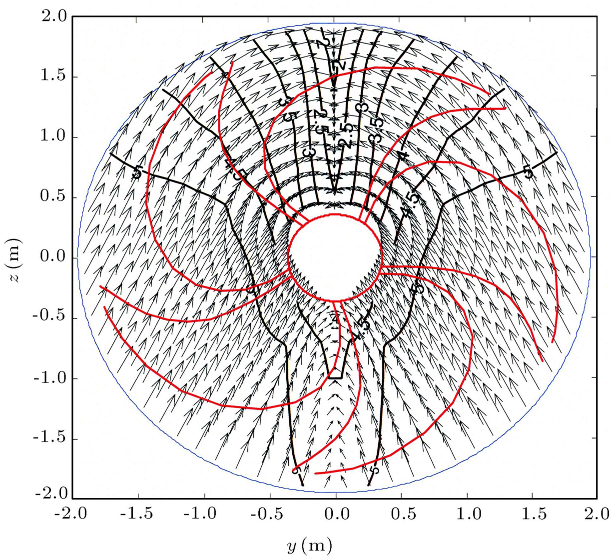

Figure 4. Contour and vector inflow wake velocity distribution for Seiun-Maru ship.

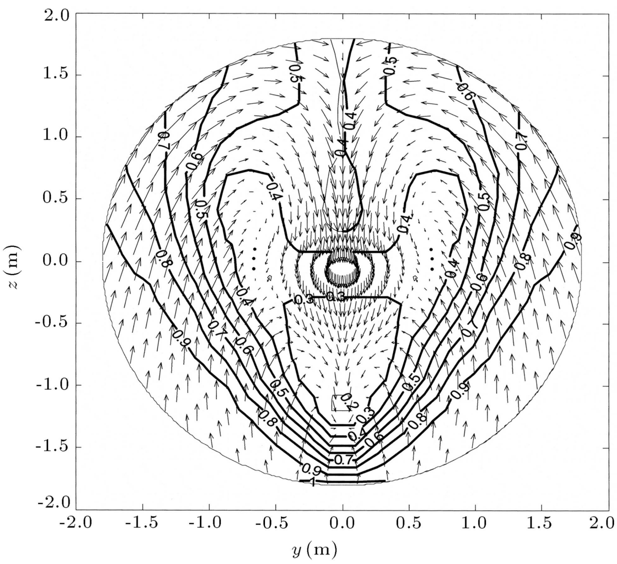

Figure 6. Contour and vector inflow wake velocity distribution behind the MS689 ship.

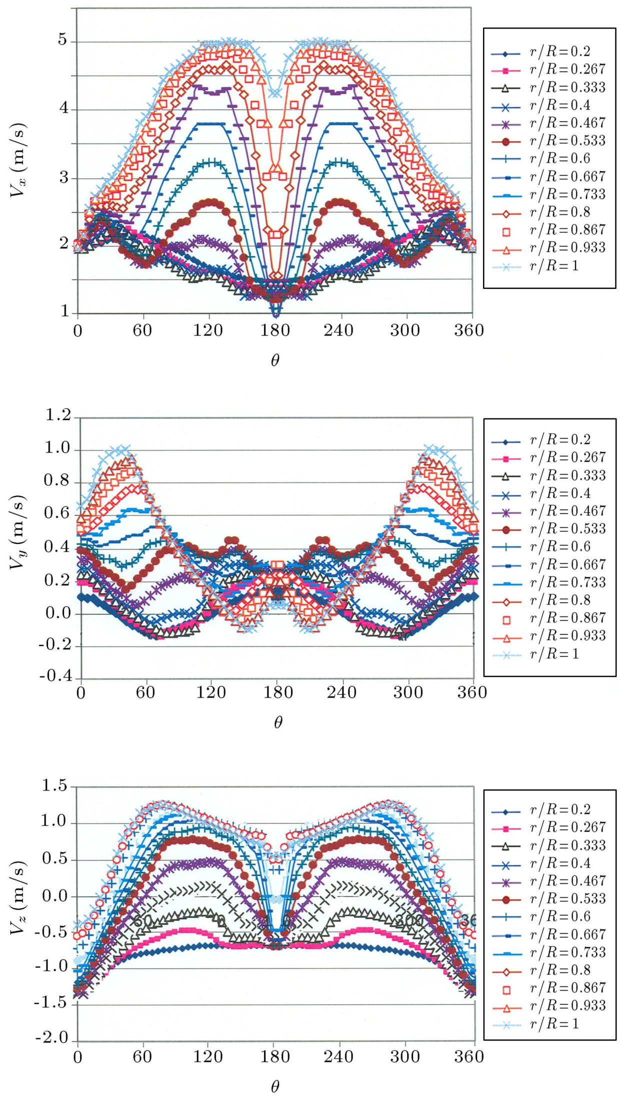

Figure 7. Interpolation of the inflow wake velocity for MS689 Ship.

elements in the chordwise and 12 elements in the radial. The hub is also divided by the total element (20*28), of which, 28 elements are in the axial and 20 elements are in the circumferential direction.

The surface of the blade pressure distribution is compared with the measured data at 0.7R and 0.9R spanwise locations on the pressure and suction sides. For the present calculation, the procedure used a K_t identity, based on ship speed, to determine the operating conditions in the calculations. The ship speed is changed until the required thrust coefficient value, $K_t = 0.172$, was achieved.

The chordwise pressure distributions, at two angular positions of 0 and 180 degrees and at 0.7R and 0.9R radial sections of the CP propeller, are compared to the experimental data, as shown in Figure 8. The present results shown in that figure indicate good agreement with experimental ones.

In Figures 9 and 10, the pressure at certain points, 0.7R and 0.9R, is plotted as a function of the blade angular position, ($0 \sim 360$). The pressure results from the present method show quite pronounced fluctuation, but the measure values are smooth in every case. The reason for this discrepancy is not known, as one might see that the correct measured wake flow is not the same as the interpolation wake flow in front of the propeller.

For the $K_t = 0.172$ condition, the calculated one blade thrust and torque is given in Figure 11, with Hoshino's results, as a function of the blade angular position (0-360 degrees) for one cycle. The angle is zero at an upright position and runs clockwise if one looks from behind. Figure 12 also shows the results for CP with the same tendency as that of the HSP, in which small humps, appearing in both K_t and K_q with the present method, may be caused by tangential inflow components, which show pronounced jumps at angular positions equal to 0 and 180 degrees. Generally, thrust and torque values of the present method are bigger at some angular positions and smaller at some others. This discrepancy is maybe due to the error in pressure distribution.

Total thrust and torque fluctuations for CP and HSP propellers are shown in Figure 13. It is clearly observed that the fluctuations of conventional propellers give significantly bigger fluctuation than highly skewed propellers under the same operating conditions. Therefore, the HSP propeller may help to avoid noise and vibration rather than the CP propeller.

Effect of Inflow Wake on the Propeller

The effect of unsteady inflow to the propeller blade, while passing through the inflow wake, causes dynamical changes in the blade pressure distribution. A decrease in pressure to a level below vapor pressure causes the water to boil locally on the propeller blade, e.g. intermittent cavitation occurs.

Due to these effects, the unsteady inflow variations are investigated on the two propellers to determine the thrust and torque during one cycle. Because of the flow, the variations of two wakes (MS689 and Seiun-Maru) are different. Therefore, in order to specify the propeller characteristics, ship speed is changed until the required thrust coefficient value, K_t, is equal for both wakes. For this reason, when the MS689 wake flow is considered for the propeller, the ship speed reaches 17.5 knots. Therefore, we operated two ship speeds (i.e. 10.7 and 17.5 knots) for both wake flows.

These two wakes flow into the CP and HSP propellers at two speeds of 10.7 and 17.5 knots. The thrust and torque fluctuating in one cycle are shown in Figures 14 and 15. It is observed that the MS689 wake

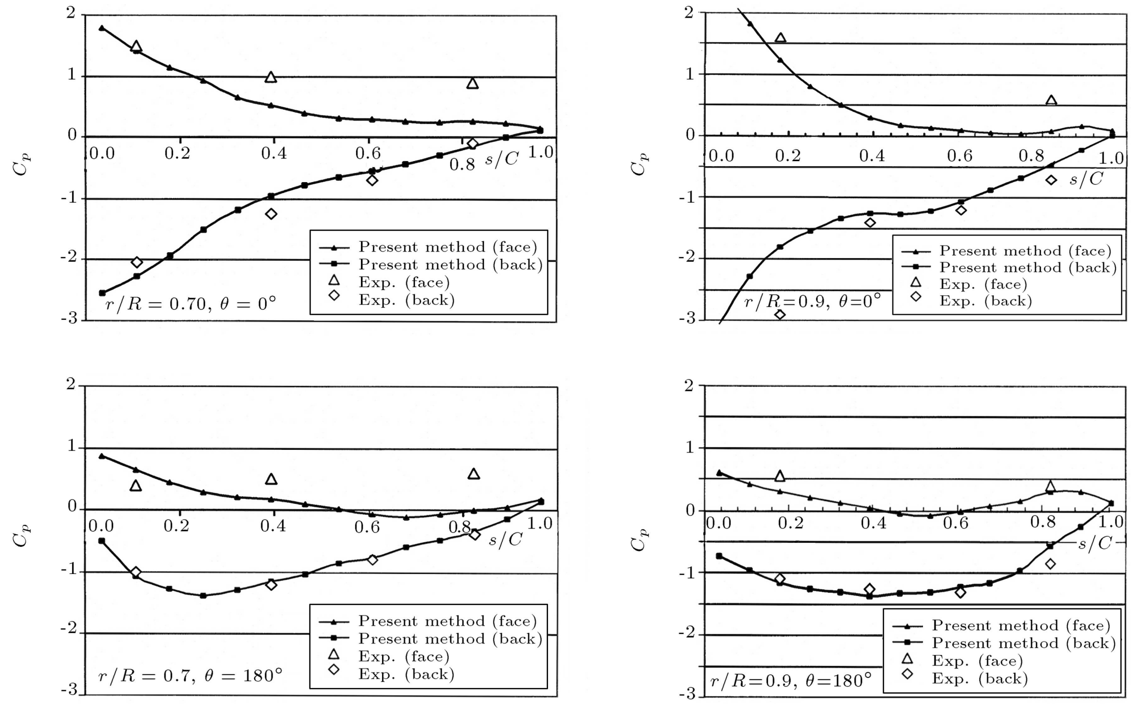

Figure 8. Comparison of chordwise pressure distribution for CP at various rotation angle, $J = 0.851$.

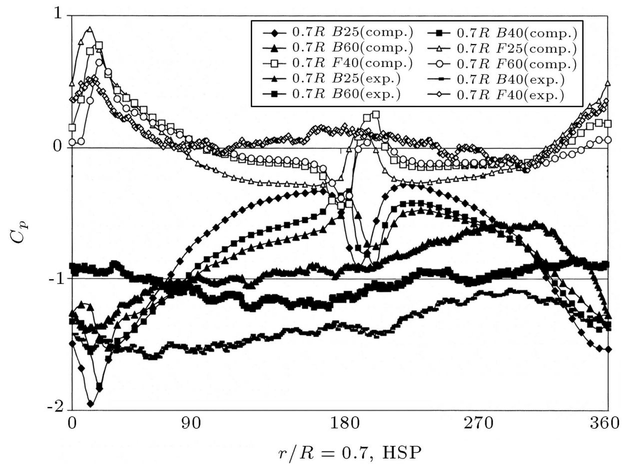

Figure 9. Fluctuating pressure for HSP on 0.7R; $K_t = 0.172$.

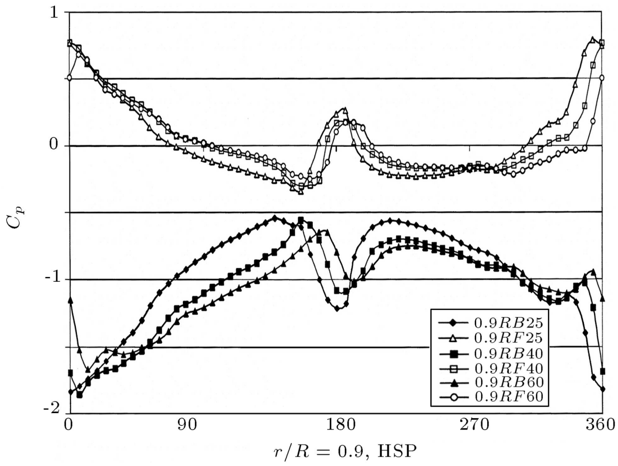

Figure 10. Fluctuating pressure for HSP on 0.9R; $K_t = 0.172$.

flow gives more fluctuating thrust and torque, relative to both propellers (CP and HSP), although it is less for the HSP propeller.

Effect of Skew Angle on the Thrust and the Torque

The numerical calculation results were extended to examine the effects of skew angle on the propeller. Figure 16 shows the propeller (the main data is the same as the HSP propeller from Table 1) with four various skew angles. The Seiun-Maru inflow wake flow is considered for the propeller and its effect is shown in Figures 17 and 18 for the thrust and torque coefficients. It is concluded that, when the propeller skew angle is increased, the domain fluctuation is decreased.

CONCLUSIONS

A potential-based BEM has been employed to analyze the hydrodynamic performance of ship propellers subject to an inflow wake. An efficient algorithm of the explicit Kutta condition (at the blade trailing edge) has been implemented, in order to ensure faster convergence at each time step. From the above numerical analysis, the following conclusions are drawn:

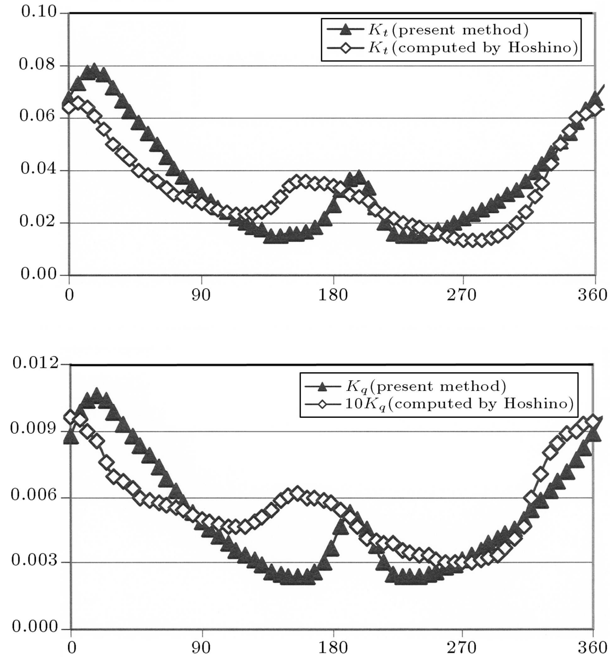

Figure 11. One blade thrust and torque fluctuations for HSP; $K_t = 0.1723$.

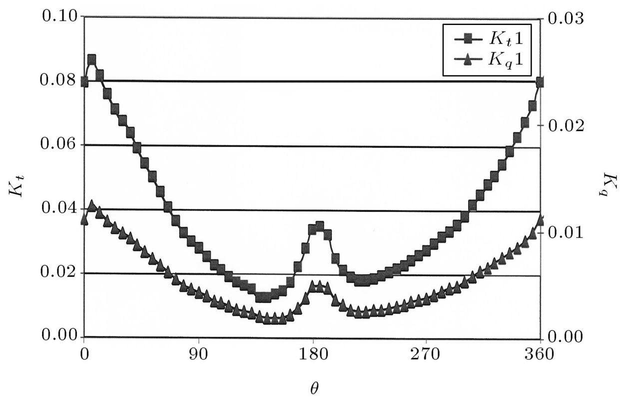

Figure 12. One blade thrust and torque fluctuations for CP; $K_t = 0.172$.

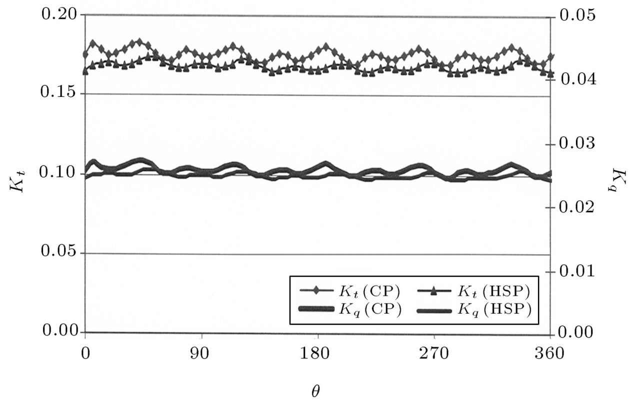

Figure 13. Total thrust and torque fluctuations for CP and HSP; $K_t = 0.172$.

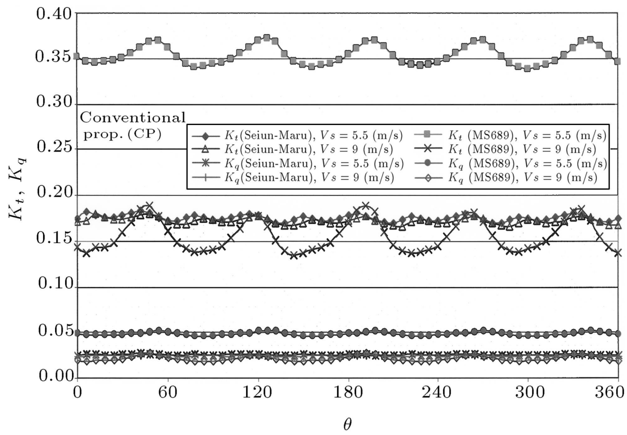

Figure 14. Comparison of total thrust and torque fluctuations for CP with two types of inflow wake.

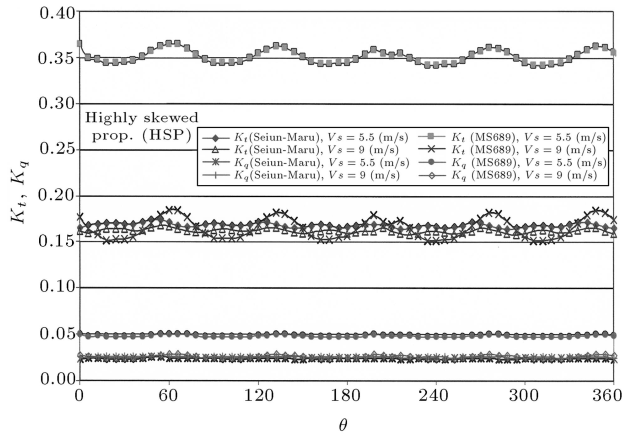

Figure 15. Comparison of total thrust and torque fluctuations for HSP with two types of inflow wake.

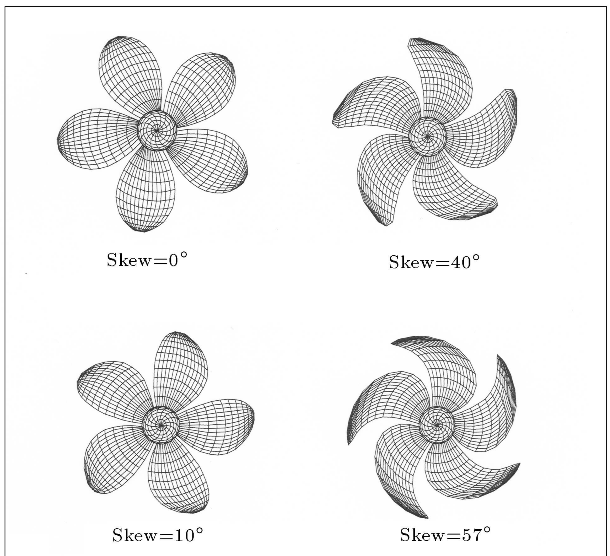

Figure 16. Element arrangement of the propellers with different skew angles.

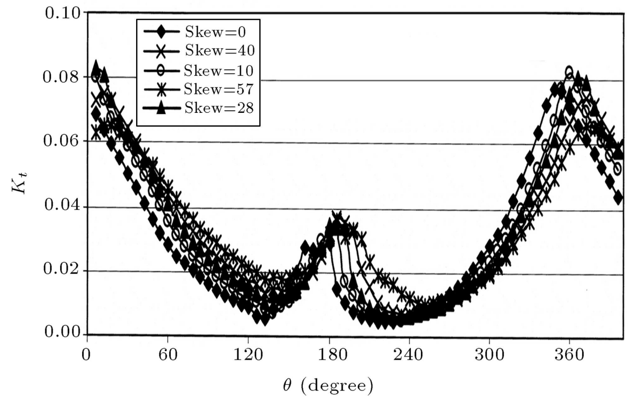

Figure 17. Effect of skew angle on thrust in one cycle.

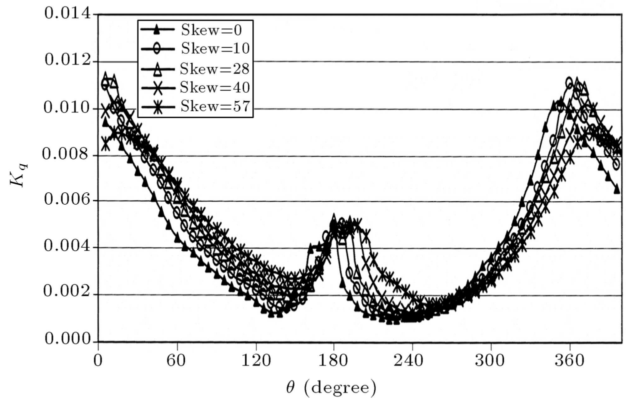

Figure 18. Effect of skew angle on torque in one cycle.

- This method may predict well, with reasonable accuracy, the effect of an inflow wake on the complicated propeller blade and obtains pressure distribution, thrust and torque fluctuation;
- The effect of skew angle is important on the hydrodynamic characteristics. It is shown that the total thrust and torque of the lower skew, like the Conventional Propeller (CP), give slightly larger fluctuations than the Highly Skewed Propeller (HSP). Therefore, the use of skew is much more important on the reduction of propeller-excited vibrations on the full-body;
- Two types of inflow wake have been introduced to conventional and highly skewed propellers. The results show large effects on propeller hydrodynamic performance by the wake flow;
- Extension research work should be considered for cavitation problems on ship propellers in unsteady conditions behind the ship hull. It is my wish to design a new propeller system for excellent operating performance.

REFERENCES

1. Kinnas, S.A. and Hsin, C.Y. "Boundary element method for the analysis of the unsteady flow around extreme propeller geometry", *Journal of AIAA*, **30**(3), pp. 688-696 (1992).
2. Hess, J.L. and Smith, A.M.O. "Calculation of non-lifting potential flow about arbitrary 3-dimensional bodies", *Journal of Ship Research*, **8**(2), pp. 22-44 (1964).
3. Morino, L., Chen, L.T. and Suciu, E.O. "Steady and oscillatory subsonic aerodynamics around complex configuration", *AIAA Journal*, **13**, pp. 368-374 (1975).
4. Lee, H. and Kinnas, S.A. "Unsteady wake alignment for propellers in nonaxisymmetric flows", *Journal of Ship Research*, **49**(3), pp. 176-190 (2005).
5. Hoshino, T. "Hydrodynamic analysis of propellers in unsteady flow using a surface element method", *J. of Society of Naval Architects of Japan*, **174**, pp. 79-92 (1993).
6. Lee, J.T. "A potential based panel method for the analysis of marine propeller in steady flow", Ph.D. Dissertation, Dept. of Ocean Eng., MIT. (1987).
7. Koyama, K. "Application of a element method to the unsteady hydrodynamic analysis of marine propellers", *Proceedings of the 19th Symposium on Naval Hydrodynamics*, Korea (1992).
8. Ghassemi, H. "Boundary element method applied to the three-dimensional cavitating hydrofoil and marine propeller", *International Journal of Scientia Iranica*, **10**(2), pp. 142-152 (2003).
9. Ghassemi, H. and Ghadimi, P. "Computational hydrodynamic analysis of the propeller-rudder and the AZIPOD systems", *J. of Ocean Engineering*, **34**(18), pp. 117-130 (2007).
10. Hsin, C.Y. "Development and analysis of panel methods for propellers in unsteady flow", Ph.D. Dissertation, Dept. of Ocean Eng., MIT (1990).
11. Felli, M., Guj, G. and Camussi, R. "Effect of the number of blades on propeller wake evolution", *Exp. Fluids*, **44**(3), pp. 409-418 (2007).
12. Felice, F., Florio, D., Felli, M. and Romano, G. "Experimental investigation of the propeller wake at different loading conditions by particle image velocimetry", *J. of Ship Research*, **48**, pp. 168-190 (2004).
13. Ukon, Y., Kudo, T., Yuasa, H. and Kamiirisa, H. "Measurement of pressure distributions on a full scale propeller-measurement on a highly skewed propeller", *Journal of Society of Naval Architects of Japan*, **170**, pp. 111-123 (1991).
14. Taylor, T.E. "Combined experimental and theoretical determination of effective wake for a marine propeller", MSc. Thesis, Department of Ocean Engineering, MIT (1994).